Role of deformation in odd-even staggering in reaction cross sections for ^{30,31,32}Ne and ^{36,37,38}Mg isotopes

Y. Urata,[1] K. Hagino,[1,2] and H. Sagawa[3,4]
[1]*Department of Physics, Tohoku University, Sendai, 980-8578, Japan*
[2]*Research Center for Electron Photon Science, Tohoku University, 1-2-1 Mikamine, Sendai 982-0826, Japan*
[3]*RIKEN Nishina Center, Wako 351-0198, Japan*
[4]*Center for Mathematics and Physics, University of Aizu, Aizu-Wakamatsu, Fukushima 965-8560, Japan*
(Received 21 October 2017; published 15 December 2017)

We discuss the role of pairing antihalo effect in the observed odd-even staggering in reaction cross sections for ^{30,31,32}Ne and ^{36,37,38}Mg isotopes by taking into account the ground-state deformation of these nuclei. To this end, we construct the ground-state density for the ^{30,31}Ne and ^{36,37}Mg nuclei based on a deformed Woods-Saxon potential, while for the ^{32}Ne and ^{38}Mg nuclei we also take into account the pairing correlation using the Hartree-Fock-Bogoliubov method. We demonstrate that, when the one-neutron separation energy is small for the odd-mass nuclei, a significant odd-even staggering still appears even with finite deformation, although the degree of staggering is somewhat reduced compared to the spherical case. This implies that the pairing antihalo effect in general plays an important role in generating the odd-even staggering in reaction cross sections for weakly bound nuclei.

DOI: 10.1103/PhysRevC.96.064311

I. INTRODUCTION

The halo structure is one of the most important phenomena in neutron-rich nuclei [1,2]. This phenomenon is characterized by a spatially extended density distribution originated from weakly bound valence neutron(s). This was first discovered by Tanihata *et al.* [3,4], who observed considerably large interaction cross sections for ^{11}Li, ^{11}Be, and ^{14}Be. Subsequently, a narrow momentum distribution was also discovered [5] for a weakly bound nucleus, ^{11}Li, establishing the concept of the halo structure. The heaviest halo nucleus discovered so far is ^{37}Mg [6,7].

For weakly bound nuclei with two valence neutrons, the pairing correlation between the valence neutrons may quench the halo structure [8]. That is, the pairing correlation alters the asymptotic behavior of the wave function for the valence neutrons, reducing the divergence feature of nuclear radii for s and p waves at zero separation energy [9–12]. This effect is referred to as the pairing antihalo effect, which can also be viewed as a generation of a spatially localized wave packet of quasiparticles originated from a coherent scattering of the valence neutrons to the continuum spectrum caused by the pairing interaction [13].

In previous publications, we have argued that the pairing antihalo effect plays an important role in the odd-even staggering observed in interaction cross sections [14–16]. That is, the experimental data have often shown a large odd-even staggering in interaction and reaction cross sections, in which cross sections for odd-mass nuclei are systematically larger than those for the neighboring even-mass nuclei [7,17]. Using the Hartree-Fock-Bogoliubov (HFB) method with spherical symmetry, we have shown that the observed odd-even staggering can be largely accounted for in terms of the pairing antihalo effect (see also Refs. [18,19]).

In this article, we extend our previous analyses by taking into account the ground-state deformation of weakly bound nuclei. To this end, we study the odd-even staggering in the ^{30,31,32}Ne and ^{36,37,38}Mg isotopes, for which the ^{31}Ne and ^{37}Mg nuclei have been suggested to have a deformed halo structure with a p wave [6,7,17,20–28].

There are two possible effects of nuclear deformation on the odd-even staggering. First, several angular momentum components are mixed in a deformed single-particle wave function for a valence neutron, reducing the s- and p-wave components in the wave function. This will reduce the radius of the ^{31}Ne and ^{37}Mg nuclei, somewhat quenching the odd-even staggering in the interaction and reaction cross sections. Second, the deformation may change the level density around the Fermi level, which would result in either an enhancement or a decrease of the pairing correlation, depending on the position of the Fermi surface. This would eventually influence the magnitude of the pairing antihalo effect, and thus the cross sections for ^{32}Ne and ^{38}Mg. The primary aim of this article is to investigate how these two effects interplay with each other in actual cases and how the conclusion obtained in our previous analyses based on spherical symmetry is altered if the deformation is explicitly taken into account.

The article is organized as follows. In Sec. II, we briefly summarize the theoretical frameworks. In our calculations, we first generate the deformed ground-state density using the HFB method with Woods-Saxon potentials, which is then used as an input to the Glauber theory to compute reaction cross sections. In Sec. III, we apply these frameworks to reaction cross sections for the ^{30,31,32}Ne and ^{36,37,38}Mg nuclei and discuss the role of deformation in the odd-even staggering in the reaction cross sections. We then summarize the article in Sec. IV.

II. THEORETICAL FRAMEWORKS

A. Deformed density

We analyze the reaction cross sections for the ^{30,31,32}Ne and ^{36,37,38}Mg nuclei. Symbolically, we denote the three isotopes

in each element as A, $A+1$, and $A+2$ systems, respectively. Our first task is to construct the ground-state density of each nucleus by taking into account the deformation. For simplicity, we ignore the pairing correlation in the A and $A+1$ systems and construct the density distribution by putting the nucleons into the lowest A and $A+1$ single-particle orbits in a deformed Woods-Saxon potential, respectively (we have confirmed that the reaction cross section for the ^{30}Ne and ^{36}Mg nuclei does not significantly change even if the pairing correlation is taken into account).

For the $A+2$ systems, on the other hand, we take into account the pairing correlation with the HFB method. In the coordinate space representation, the HFB equations read [29–31]

$$\begin{pmatrix} \hat{h}-\lambda & \Delta(\boldsymbol{r}) \\ \Delta(\boldsymbol{r}) & -\hat{h}+\lambda \end{pmatrix} \begin{pmatrix} U_i(\boldsymbol{r}) \\ V_i(\boldsymbol{r}) \end{pmatrix} = E_i \begin{pmatrix} U_i(\boldsymbol{r}) \\ V_i(\boldsymbol{r}) \end{pmatrix}, \tag{1}$$

where $\Delta(\boldsymbol{r})$ is the pairing potential, and λ and E_i are the chemical potential and a quasiparticle energy, respectively. $\hat{h}$ is a mean-field Hamiltonian given by

$$\hat{h} = -\frac{\hbar^2}{2m}\nabla^2 + V(\boldsymbol{r}), \tag{2}$$

where $V(\boldsymbol{r})$ is a mean-field potential and m is the nucleon mass. Here, we have assumed that the nucleon-nucleon interaction is zero range, so that the mean-field potential and the pairing potential are both local. In this framework, the density distribution is given by

$$\rho(\boldsymbol{r}) = \sum_i |V_i(\boldsymbol{r})|^2. \tag{3}$$

The chemical potential λ is determined so that the average particle number is $A+2$, that is,

$$\int d\boldsymbol{r}\,\rho(\boldsymbol{r}) = A+2. \tag{4}$$

For simplicity, we use a deformed Woods-Saxon potential for $V(\boldsymbol{r})$ and $\Delta(\boldsymbol{r})$ given by

$$V(\boldsymbol{r}) = V_0\left(f(r) - R_0\beta_2\frac{df(r)}{dr}Y_{20}(\theta_{rd})\right) + V_{\rm ls}\frac{1}{r}\frac{df(r)}{dr}(\boldsymbol{l}\cdot\boldsymbol{s}), \tag{5}$$

$$\Delta(\boldsymbol{r}) = \Delta_0\left(f(r) - R_0\beta_2\frac{df(r)}{dr}Y_{20}(\theta_{rd})\right), \tag{6}$$

with

$$f(r) = \frac{1}{1+\exp[(r-R_0)/a]}. \tag{7}$$

Here, we have assumed axially symmetric quadrupole deformation with the deformation parameter of β_2 and denoted the angle between the vector $\boldsymbol{r}$ and the symmetry axis as θ_{rd}. In the single-particle potential, we take into account only the spherical part of the spin-orbit potential. For the protons, we also add the spherical Coulomb interaction to the mean-field potential, Eq. (5), with the radius of R_0.

We use the same values for the parameters for the single-particle potential as those listed in Table I in Ref. [32], except for the depth parameter V_0 for the configuration for the valence orbit, for which we adjust the value of V_0 so that the neutron separation energy for the $A+1$ nuclei is reproduced. For simplicity, we use the same value for the deformation parameter for all three isotopes, A, $A+1$, and $A+2$. For the strength Δ_0 for the neutron pairing potential, Eq. (6), we determine it according to

$$\bar{\Delta} \equiv \frac{\int d\boldsymbol{r}\,\Delta(\boldsymbol{r})f(r)}{\int d\boldsymbol{r}\,f(r)}, \tag{8}$$

with the average pairing gap of $\bar{\Delta} = 12/\sqrt{A+2}$ MeV. For the protons, we ignore the pairing correlation as they are deeply bound in the nuclei considered in this article, and thus the effect of pairing correlation on the nuclear radius is expected to be small.

We solve the HFB equations, Eqs. (1), by expanding the upper and the lower components of the quasiparticle wave functions as

$$U_K(\boldsymbol{r}) = \sum_{n,l,j} u_{nlj}\,\psi_{nljK}(\boldsymbol{r}), \tag{9}$$

$$V_K(\boldsymbol{r}) = \sum_{n,l,j} v_{nlj}\,\psi_{nljK}(\boldsymbol{r}), \tag{10}$$

where $\{\psi_{nljK}(\boldsymbol{r})\}$ are eigenfunctions of the single-particle Hamiltonian $\hat{h}$ when the deformation parameter β_2 is set to zero. This wave function is characterized by the radial quantum number n, the orbital angular momentum l, the total single-particle angular momentum j, and its projection onto the symmetry axis, K. Notice that K is conserved in the quasiparticle wave functions, since we assume the axial symmetry. In Eqs. (9) and (10), we include the continuum states up to 30 MeV above the Fermi energy λ by discretizing them with the box boundary condition at $R_{\rm box} = 60$ fm.

B. Reaction cross sections

We next consider collision of a deformed projectile nucleus with a spherical target nucleus and compute the reaction cross sections σ_R. To this end, we employ the Glauber theory, which is based on the eikonal approximation and the adiabatic approximation to the nucleonic motions [33,34]. To calculate reaction cross sections, we also apply the adiabatic approximation to the rotational motion of a deformed nuclei. That is, we first fix the orientation angle of the deformed nucleus and then take an average of the resultant cross section over all the orientation angles [35,36]. The reaction cross sections are thus expressed as

$$\sigma_R = \frac{1}{4\pi}\int d\boldsymbol{\Omega}\,\sigma_R(\boldsymbol{\Omega}), \tag{11}$$

where $\boldsymbol{\Omega}$ is the angle of the symmetric axis of the deformed nucleus in the laboratory frame, and $\sigma_R(\boldsymbol{\Omega})$ is the reaction cross section for fixed $\boldsymbol{\Omega}$.

In the Glauber theory, the reaction cross section is computed as [37–42]

$$\sigma_R(\boldsymbol{\Omega}) = \int d\boldsymbol{b}(1 - |e^{i\chi(\boldsymbol{b},\boldsymbol{\Omega})}|^2), \tag{12}$$

where $\boldsymbol{b}$ is the impact parameter and the phase shift function χ is given by

$$i\chi(\boldsymbol{b};\boldsymbol{\Omega}) = -\int d\boldsymbol{r}\,\rho_P(\boldsymbol{r};\boldsymbol{\Omega}) \times\left[1-\exp\left(-\int d\boldsymbol{r}'\rho_T(\boldsymbol{r}')\,\Gamma_{NN}(\boldsymbol{s}-\boldsymbol{s}'+\boldsymbol{b})\right)\right]. \tag{13}$$

Here, $\boldsymbol{s}$ and $\boldsymbol{s}'$ are the transverse components (that is, the component which is parallel to $\boldsymbol{b}$) of $\boldsymbol{r}$ and $\boldsymbol{r}'$, respectively. Γ_{NN} is the profile function for the NN scattering, which we assume to be [37–42]

$$\Gamma_{NN}(\boldsymbol{b}) = \frac{1-i\alpha}{4\pi\beta}\sigma_{NN}\exp\left(-\frac{b^2}{2\beta}\right), \tag{14}$$

where σ_{NN} is the total NN cross section. In Eq. (13), ρ_P and ρ_T are the density distributions for the projectile and the target nuclei, respectively. We assume that the target density is spherical, $\rho_T(\boldsymbol{r}) = \rho_T(r)$, while the projectile density has axial symmetry, that is,

$$\rho_P(\boldsymbol{r};\boldsymbol{\Omega}) = \rho_P(r,\theta_{rd}). \tag{15}$$

The projectile density can be expanded into multipoles as

$$\rho_P(r,\theta_{rd}) = \sum_\lambda \rho_\lambda^{(P)}(r)Y_{\lambda 0}(\theta_{rd}), \tag{16}$$

$$= \sum_{\lambda,\mu}\sqrt{\frac{4\pi}{2\lambda+1}}\,\rho_\lambda^{(P)}(r)Y_{\lambda\mu}(\hat{\boldsymbol{r}})Y^*_{\lambda\mu}(\boldsymbol{\Omega}). \tag{17}$$

Notice that the phase shift function given by Eq. (13) takes into account the effect beyond the optical-limit approximation following the prescription proposed in Ref. [43]. We evaluate it using the Fourier transform method [15,44].

In this article, we analyze the experimental data at incident energy $E = 240$ MeV/nucleon with ^{12}C target [7,17]. We use the same density for ^{12}C as that given in Ref. [38], while we use the same parameters given in Ref. [45] for the profile function Γ_{NN}.

III. ODD-EVEN STAGGERING IN REACTION CROSS SECTIONS

A. ^{30,31,32}Ne isotopes

Let us now numerically evaluate the reaction cross section for deformed nuclei and discuss the role of deformation in the odd-even staggering in the reaction cross sections. We first consider the ^{30,31,32}Ne isotopes, for which the odd-even staggering has been investigated assuming spherical symmetry [14].

In Ref. [24], we have shown that the measured reaction cross section for the ^{31}Ne nucleus can be reproduced both with the particle-rotor model and with the Nilsson model with a deformed Woods-Saxon potential when the quadrupole deformation parameter is in the range of $0.17 \leqslant \beta_2 \leqslant 0.33$. In this case, the valence neutron in ^{31}Ne occupies the [330 1/2] ($K^\pi = 1/2^-$) orbit, which is connected to the $1f_{7/2}$ level in the spherical limit [22]. In this article, we therefore choose $\beta_2 = 0.3$. As has been demonstrated in Ref. [24], the dependence of reaction cross sections on the deformation parameter is weak once the configuration of the valence orbit is fixed.

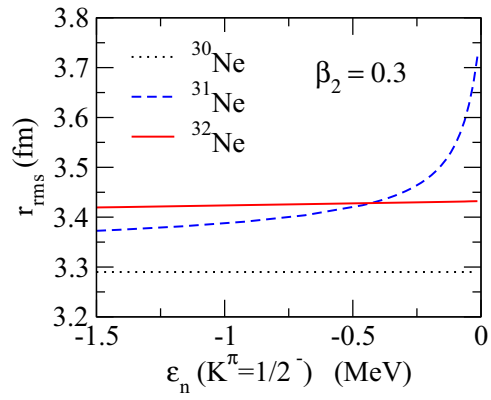

FIG. 1. The root-mean-square radius for the ^{30,31,32}Ne isotopes as a function of the one-neutron separation energy of the ^{31}Ne nucleus. The dotted, the dashed, and the solid lines indicate the radius of the ^{30}Ne, ^{31}Ne, and ^{32}Ne nuclei, respectively. The pairing correlation is taken into account only in the ^{32}Ne nucleus using the Hartree-Fock-Bogoliubov method. The deformation parameter is set to be $\beta_2 = 0.3$ for all the three nuclei so that the valence neutron in ^{31}Ne occupies the $K^\pi = 1/2^-$ orbit. The figure is obtained by varying the depth parameter in the single-particle potential for the $K^\pi = 1/2^-$ configuration.

Figure 1 shows the root-mean-square radii so obtained for the ^{30,31,32}Ne nuclei as a function of the energy of the valence orbit for the ^{31}Ne nucleus, ϵ_n. To draw this figure, we vary the depth parameter V_0 in the Woods-Saxon potential for the $K^\pi = 1/2^-$ configuration. The dotted, the dashed, and the solid lines show the radius for the ^{30}Ne, ^{31}Ne, and ^{32}Ne nuclei, respectively. One can see that the radius of the ^{31}Ne increases rapidly as the one-neutron separation energy, $S_n = -\epsilon_n$, approaches zero, due to the p-wave component in the wave function for the valence neutron. On the other hand, the radius of the ^{32}Ne nucleus varies slowly as a function of the one-neutron separation energy and becomes smaller than that of the ^{31}Ne nucleus for $\epsilon_n \leqslant -0.42$ MeV due to the pairing antihalo effect. This behavior is qualitatively the same as in the previous analysis shown in the middle panel of Fig. 2 in Ref. [14], which was based on the spherical symmetry of the Ne isotopes.

The reaction cross sections for the ^{30,31,32}Ne nuclei evaluated at $S_n(^{31}\text{Ne}) = 0.3$ MeV are shown in Fig. 2. These are compared with the experimental interaction cross sections [17], which are expected to be close to the reaction cross sections for neutron-rich nuclei [7,38,46]. For comparison, we also show the result of the previous analysis [14] at a similar one-neutron separation energy, even though the single potential is different from the one used in the present analysis. One can see that the odd-even staggering can still be reproduced by taking into account the nuclear deformation. Notice that the degree of the staggering becomes smaller in the present calculation compared to the previous spherical calculation. This is because the valence neutron in ^{31}Ne

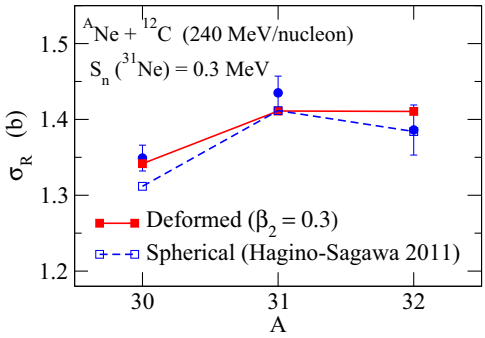

FIG. 2. The reaction cross sections for the ^{30,31,32}Ne + ^{12}C reaction at $E = 240$ MeV/nucleon. These are evaluated at the one-neutron separation energy of ^{31}Ne of $S_n = 0.3$ MeV. The solid circles with error bars indicate the experimental interaction cross sections taken from Ref. [17]. For comparison, the results of the previous analysis (Hagino-Sagawa [14]) based on the spherical density distributions are also shown by the dashed line.

fully occupies the $1p_{3/2}$ level in the spherical case, while the occupation probability for the $p_{3/2}$ level decreases from unity in the deformed case. In the case shown in Fig. 2, our calculation yields the occupation probability of 46.3%.

A larger staggering can be obtained with deformation when the one-neutron separation energy of ^{31}Ne is further decreased. To demonstrate this, Fig. 3 shows the staggering parameter γ_3 defined as [15]

$$\gamma_3 \equiv \frac{(-1)^A}{2}[\sigma_R(A+1) - 2\sigma_R(A) + \sigma_R(A-1)], \qquad (18)$$

where $\sigma_R(A)$ is the reaction cross section of a nucleus with mass number A. The dashed and the solid lines in the figure show the staggering parameter for the spherical and the deformed cases, respectively. For a fixed value of separation energy, the staggering parameter γ_3 is smaller in the deformed case as compared to the spherical case, which is consistent with Fig. 2. However, the staggering parameter increases as

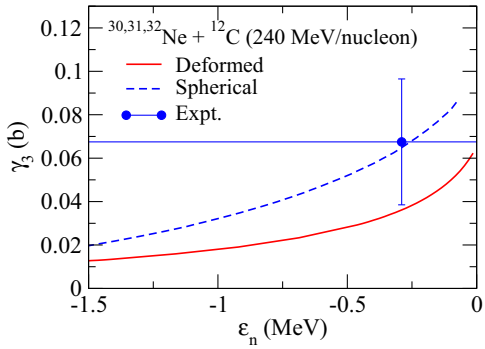

FIG. 3. The staggering parameter γ_3 defined by Eq. (18) for the ^{30,31,32}Ne + ^{12}C reactions at $E = 240$ MeV/nucleon. It is plotted as a function of the single-particle energy for the valence orbit for the ^{31}Ne nucleus. The dashed and the solid lines are obtained using the spherical and the deformed density distributions, respectively. The experimental data are evaluated using the measured interaction cross sections shown in Ref. [17].

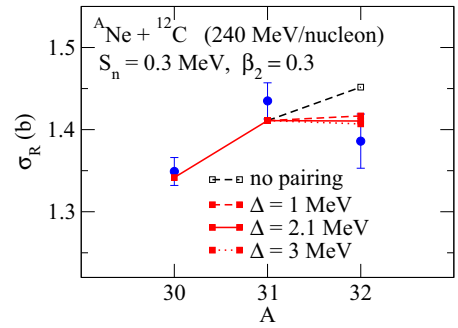

FIG. 4. The dependence of the reaction cross section for the ^{32}Ne nucleus on the average pairing gap. The solid squares with the dashed, the solid, and the dotted lines are obtained by setting the average pairing gap to be 1, 2.1 ($=12/\sqrt{32}$), and 3 MeV, respectively. For comparison, the open square with the dashed line shows the result without the pairing correlation.

the separation energy decreases, and eventually comes closer to the central value of the experimental data when ϵ_n is around the threshold.

In Sec. I, we have conjectured that the nuclear deformation may lead to two effects on reaction cross sections. One is to decrease the cross section for ^{31}Ne due to the admixture of several angular momentum components in the single-particle wave function for the valence orbit. The other is to change the cross section for ^{32}Ne because of a change in the degree of pairing antihalo effect. The former effect would reduce the staggering, while the latter effect either enhances or reduces it depending on the level density around the Fermi surface. Our calculation shown in Fig. 2 indicates that the former effect indeed exists, while the latter effect is much less clear. To shed light on the latter effect, Fig. 4 shows the dependence of the reaction cross section on the strength of the pairing correlation. To this end, we vary the average pairing gap, $\bar{\Delta}$, defined by Eq. (8). The solid squares with the dashed, the solid, and the dotted lines are obtained by setting the average pairing gap to be 1, 2.1 ($=12/\sqrt{32}$), and 3 MeV, respectively. Notice that the solid line is the same as that in Fig. 2. For comparison, the open square with the dashed line shows the results without the pairing correlation. One can clearly see that the reaction cross section for ^{32}Ne is not sensitive to the value of the average pairing gap as long as it is large enough. This would be correlated to the fact that the root-mean-square radius for ^{32}Ne is not sensitive to the single-particle energy for the valence orbit of ^{31}Ne, as has been shown in Fig. 1. Even though the occupation probability for the p-wave orbital may depend largely on the average pairing gap, the root-mean-square radius does not change much once the radius is significantly shrunken due to the pairing antihalo effect so that the s- and p-wave states do not behave abnormally. This indicates that the main effect of nuclear deformation is simply to decrease the odd-even staggering in reaction cross sections, at least for the Ne isotopes.

B. ^{36,37,38}Mg isotopes

Let us next discuss the ^{36,37,38}Mg isotopes. For ^{37}Mg in these isotopes, the p-wave halo structure has been suggested from a measurement of the one-neutron removal reaction on C

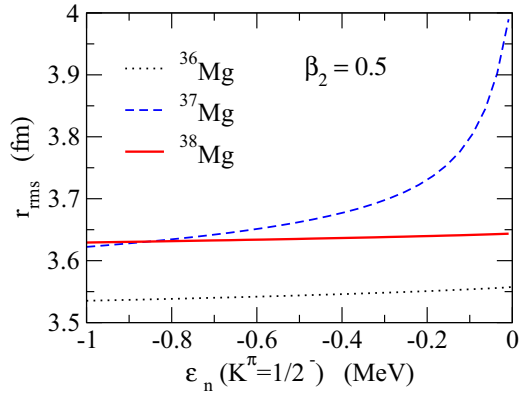

FIG. 5. Same as Fig. 1, but for the ^{36,37,38}Mg isotopes.

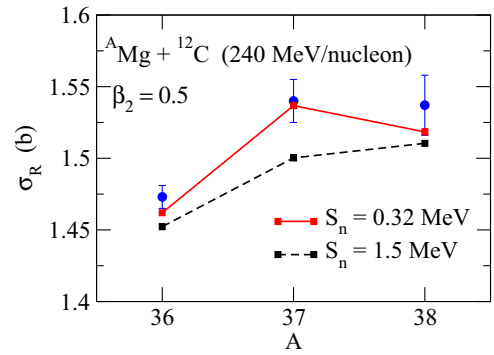

FIG. 6. The reaction cross sections for the ^{36,37,38}Mg + ^{12}C reaction at $E = 240$ MeV/nucleon. These are evaluated for the quadrupole deformation parameter of $\beta_2 = 0.5$, at which the valence neutron in ^{37}Mg occupies the [321,1/2] orbital. The solid and the dashed lines denote the results for $S_n = 0.32$ and 1.5 MeV, respectively, where S_n is the one-neutron separation energy of ^{37}Mg. The experimental reaction cross sections are taken from Ref. [7].

and Pb targets, with a small one-neutron separation energy of $0.22^{+0.12}_{-0.09}$ MeV [6]. Moreover, the experimental reaction cross sections indicate a large odd-even staggering for ^{36,37,38}Mg [7].

We first determine the deformation parameter β_2 for these isotopes. With the deformed Woods-Saxon potential shown in Sec. II A, together with the parameters listed in Table I in Ref. [32], we find that the valence neutron in ^{37}Mg occupies the [312 5/2] orbit for $\beta_2 \leqslant 0.4$, while it occupies the [321 1/2] orbit for $0.4 \leqslant \beta_2 \leqslant 0.6$. The former is connected to the $1f_{7/2}$ level while the latter is connected to the $2p_{3/2}$ level in the spherical limit. The former state has $K^\pi = 5/2^-$, and thus contains angular momenta larger than $l = 3$, which do not form a halo structure. In contrast, the latter state contains a large p-wave component, being consistent with the suggested halo structure for ^{37}Mg [7]. We therefore choose $\beta_2 = 0.5$ in the analysis shown below.

Figure 5 shows the root-mean-square radii for the ^{36,37,38}Mg nuclei as a function of the single-particle energy for the valence orbit of ^{37}Mg. The radii behave qualitatively the same as those for the Ne isotopes shown in Fig. 1. That is, the radius of ^{37}Mg diverges in the limit of vanishing single-particle energy, while that of ^{38}Mg varies much more slowly due to the pairing antihalo effect.

The reaction cross sections for the ^{36,37,38}Mg isotopes are shown in Fig. 6 for two different values of the one-neutron separation energy S_n for ^{37}Mg. The solid line is obtained with $S_n = 0.32$ MeV, while the dashed line is obtained with $S_n = 1.5$ MeV. The experimental odd-even staggering can be well reproduced with $S_n = 0.32$ MeV. On the other hand, for $S_n = 1.52$ MeV, the reaction cross section increases monotonically as a function of the mass number, which is inconsistent with the experimental data. Notice that this behavior is qualitatively similar to the odd-even staggering for the Ne isotopes shown in Fig. 3 in Ref. [14] obtained with the spherical densities. Therefore it is evident that the pairing antihalo effect plays an important role in the odd-even staggering of deformed neutron-rich nuclei, such as ^{30,31,32}Ne and ^{36,37,38}Mg isotopes.

IV. SUMMARY

We have investigated the role of nuclear deformation in the odd-even staggering observed in reaction cross sections for several systems. To this end, we have used the deformed Hartree-Fock-Bogoliubov method to take into account both the deformation and the pairing effects. We have applied this method to the ^{30,31,32}Ne and ^{36,37,38}Mg isotopes and have shown that the deformation mainly decreases the degree of odd-even staggering due to the admixture of several angular momentum states in a deformed single-particle wave function. Despite this, the odd-even staggering persists even with finite deformation, when the one-neutron separation energy is small enough. In particular, we have successfully accounted for the experimental odd-even staggering for both the ^{30,31,32}Ne and ^{36,37,38}Mg isotopes within the unified theoretical framework. This strongly indicates that the pairing antihalo effect indeed has a responsibility to the observed odd-even staggering in reaction cross sections.

Our calculation can be improved in several ways. For instance, in this article, we have assumed that the deformation parameter is the same for the three nuclei within the same element. It might be important to take into account an isotope-dependent deformation, as has been predicted, e.g., by the antisymmetrized molecular dynamics [25–28], although the dependence of the reaction cross sections on the deformation would not be large once the single-particle configuration is fixed. Another issue is the treatment of pairing for the odd-mass nuclei. For simplicity, in this article we have neglected the pairing correlation in ^{30,31}Ne and ^{36,37}Mg, because the effect of the pairing on the radius of ^{30}Ne and ^{36}Mg turned out to be small. However, if one regards ^{31}Ne and ^{37}Mg as one quasiparticle excitation on top of ^{32}Ne and ^{38}Mg, the pairing might play some role in these nuclei as well. A more consistent way towards this end would be to treat the odd-mass nuclei using the blocked HFB method [47,48]; that would be an interesting future work.

ACKNOWLEDGMENTS

This work was partly supported by JSPS KAKENHI Grants No. 16H02179 and No. JP16K05367.

[1] I. Tanihata, H. Savajols, and R. Kanungo, Prog. Part. Nucl. Phys. **68**, 215 (2013).

[2] K. Hagino, I. Tanihata, and H. Sagawa, in *100 Years of Subatomic Physics*, edited by E. M. Henley and S. D. Ellis (World Scientific, Singapore, 2013), p. 231.

[3] I. Tanihata, H. Hamagaki, O. Hashimoto, Y. Shida, N. Yoshikawa, K. Sugimoto, O. Yamakawa, T. Kobayashi, and N. Takahashi, Phys. Rev. Lett. **55**, 2676 (1985).

[4] I. Tanihata *et al.*, Phys. Lett. B **206**, 592 (1988).

[5] T. Kobayashi, O. Yamakawa, K. Omata, K. Sugimoto, T. Shimoda, N. Takahashi, and I. Tanihata, Phys. Rev. Lett. **60**, 2599 (1988).

[6] N. Kobayashi *et al.*, Phys. Rev. Lett. **112**, 242501 (2014).

[7] M. Takechi *et al.*, Phys. Rev. C **90**, 061305(R) (2014).

[8] K. Bennaceur, J. Dobaczewski, and M. Ploszajczak, Phys. Lett. B **496**, 154 (2000).

[9] K. Riisager, A. S. Jensen, and P. Møller, Nucl. Phys. A **548**, 393 (1992).

[10] A. S. Jensen, K. Riisager, D. V. Fedorov, and E. Garrido, Rev. Mod. Phys. **76**, 215 (2004).

[11] H. Sagawa, Phys. Lett. B **286**, 7 (1992).

[12] H. Sagawa and K. Hagino, Eur. Phys. J. A **51**, 102 (2015).

[13] K. Hagino and H. Sagawa, Phys. Rev. C **95**, 024304 (2017).

[14] K. Hagino and H. Sagawa, Phys. Rev. C **84**, 011303(R) (2011).

[15] K. Hagino and H. Sagawa, Phys. Rev. C **85**, 014303 (2012).

[16] K. Hagino and H. Sagawa, Phys. Rev. C **85**, 037604 (2012).

[17] M. Takechi *et al.*, Phys. Lett. B **707**, 357 (2012).

[18] S. Sasabe, T. Matsumoto, S. Tagami, N. Furutachi, K. Minomo, Y. R. Shimizu, and M. Yahiro, Phys. Rev. C **88**, 037602 (2013).

[19] T. Matsumoto and M. Yahiro, Phys. Rev. C **90**, 041602(R) (2014).

[20] T. Nakamura *et al.*, Phys. Rev. Lett. **103**, 262501 (2009).

[21] T. Nakamura *et al.*, Phys. Rev. Lett. **112**, 142501 (2014).

[22] I. Hamamoto, Phys. Rev. C **81**, 021304(R) (2010).

[23] Y. Urata, K. Hagino, and H. Sagawa, Phys. Rev. C **83**, 041303(R) (2011).

[24] Y. Urata, K. Hagino, and H. Sagawa, Phys. Rev. C **86**, 044613(R) (2012).

[25] K. Minomo, T. Sumi, M. Kimura, K. Ogata, Y. R. Shimizu, and M. Yahiro, Phys. Rev. C **84**, 034602 (2011).

[26] K. Minomo, T. Sumi, M. Kimura, K. Ogata, Y. R. Shimizu, and M. Yahiro, Phys. Rev. Lett. **108**, 052503 (2012).

[27] T. Sumi, K. Minomo, S. Tagami, M. Kimura, T. Matsumoto, K. Ogata, Y. R. Shimizu, and M. Yahiro, Phys. Rev. C **85**, 064613 (2012).

[28] S. Watanabe, K. Minomo, M. Shimada, S. Tagami, M. Kimura, M. Takechi, M. Fukuda, D. Nishimura, T. Suzuki, T. Matsumoto, Y. R. Shimizu, and M. Yahiro, Phys. Rev. C **89**, 044610 (2014).

[29] J. Dobaczewski, W. Nazarewicz, T. R. Werner, J. F. Berger, C. R. Chinn, and J. Dechargé, Phys. Rev. C **53**, 2809 (1996).

[30] J. Dobaczewski, H. Flocard, and J. Treiner, Nucl. Phys. A **422**, 103 (1984).

[31] A. Bulgac, arXiv:nucl-th/9907088.

[32] T. Shoji and Y. R. Shimizu, Prog. Theor. Phys. **121**, 319 (2009).

[33] R. J. Glauber, in *Lectures in Theoretical Physics*, edited by W. E. Brittin (Interscience, New York, 1959), Vol. 1, p. 315.

[34] C. A. Bertulani and P. Danielewicz, *Introduction to Nuclear Reactions* (IOP, Bristol, UK, 2004).

[35] J. A. Christley and J. A. Tostevin, Phys. Rev. C **59**, 2309 (1999).

[36] K. Hagino and N. Takigawa, Prog. Theor. Phys. **128**, 1061 (2012).

[37] Y. Ogawa, T. Kido, K. Yabana, and Y. Suzuki, Prog. Theor. Phys. Suppl. **142**, 157 (2001).

[38] Y. Ogawa, K. Yabana, and Y. Suzuki, Nucl. Phys. A **543**, 722 (1992).

[39] W. Horiuchi, Y. Suzuki, B. Abu-Ibrahim, and A. Kohama, Phys. Rev. C **75**, 044607 (2007).

[40] W. Horiuchi, Y. Suzuki, P. Capel, and D. Baye, Phys. Rev. C **81**, 024606 (2010).

[41] W. Horiuchi, T. Inakura, T. Nakatsukasa, and Y. Suzuki, Phys. Rev. C **86**, 024614 (2012).

[42] W. Horiuchi, S. Hatakeyama, S. Ebata, and Y. Suzuki, Phys. Rev. C **93**, 044611 (2016).

[43] B. Abu-Ibrahim and Y. Suzuki, Phys. Rev. C **61**, 051601(R) (2000); **62**, 034608 (2000).

[44] C. A. Bertulani and H. Sagawa, Nucl. Phys. A **588**, 667 (1995).

[45] B. Abu-Ibrahim, W. Horiuchi, A. Kohama, and Y. Suzuki, Phys. Rev. C **77**, 034607 (2008).

[46] A. Kohama, K. Iida, and K. Oyamatsu, Phys. Rev. C **78**, 061601(R) (2008).

[47] B. Bally, B. Avez, M. Bender, and P.-H. Heenen, Phys. Rev. Lett. **113**, 162501 (2014).

[48] T. T. Sun, M. Matsuo, Y. Zhang, and J. Meng, arXiv:1310.1661.